Femtosecond laser structuring and optical properties of a silver and zinc phosphate glass

Kevin Bourhis, Arnaud Royon, Matthieu Bellec, Jiyeon Choi, Alexandre Fargues, Mona Tréguer-Delapierre, Jean-Jacques Videau, David Talaga, Martin Richardson, Thierry Cardinal, et al.

Femtosecond laser structuring and optical properties of a silver and zinc phosphate glass

Kevin Bourhis [a], Arnaud Royon [b], Matthieu Bellec [b], Jiyeon Choi [a d], Alexandre Fargues [a], Mona Treguer [a], Jean-Jacques Videau [a], David Talaga [c], Martin Richardson [d], Thierry Cardinal [a], Lionel Canioni [b]

[a] *Institut de Chimie de la Matière Condensée de Bordeaux, UPR 9048 CNRS, Université de Bordeaux, 87 Avenue du Docteur Albert Schweitzer, 33608 Pessac Cedex, France*
[b] *Centre de Physique Moléculaire Optique et Hertzienne, UMR 5798 CNRS, Université de Bordeaux, 351 Cours de la Libération, 33405 Talence Cedex, France*
[c] *Institut des Sciences Moléculaires, UMR 5255 CNRS, Université Bordeaux, 351 cours de la Libération, 33405 Talence Cedex, France*
[d] *CREOL – College of Optics and Photonics, University of Central Florida, 4000 Central Florida Boulevard, Orlando, Florida 32816, USA*

Abstract

We report on the micro- and nano-structuring of a silver-containing zinc phosphate glass under high repetition rate femtosecond near-infrared laser exposure. Luminescent silver clusters are locally formed thanks to multi-photon absorption. The excitation mechanisms in the glass are investigated with a transient absorption pump-probe experiment. The free electron density of the femtosecond-laser-induced ionized material for irradiation conditions leading to structural modifications is measured. We show that the involved photo-excitation process in the laser–glass interaction is a four-photon absorption and the measured free electron density is on the order of 10^{17} cm^{-3}, four orders of magnitude below the critical electron density. The luminescence properties of these resulting structures have been investigated. Emission spectra are compared with those collected after different irradiations (γ and electron beams). The migration of silver species has been assigned to be responsible for local modifications and selective acid etching behavior of the structure.

Keywords : Silver clusters ; Luminescence ; Multiphoton absorption ; Femtosecond laser writing

1. Introduction

The development of photonics requires multiple new optical materials, in particular transparent composite materials in which photonic structures can be implemented. Glasses are materials of interest because of their transparency in a large wavelength domain from IR to UV and the possibility to use them as starting materials for implementing complex optical structures. Moreover, glasses containing noble metal (silver, copper and gold) have been reported to be good candidates for applications such as waveguides [1], nanogratings [2,3], micro-lenses [4] three-dimensional data storage [5,6] and biosensors [7]. For example silver-containing glasses have been used as photographic media [8,9] and as dosimeters for γ and X radiations [10–13]. However in most of the cases, a permanent modification of the chemical structure of the glass occurs after exposure.

Very recently, Bellec et al. reported the fabrication of luminescent structures by femtosecond laser writing in a silver-containing zinc phosphate glass [14]. The photo-induced structures present a size well below the diffraction limit. The luminescence of these structures is attributed to silver clusters located in the wall of the structures. The mechanisms of formation of these clusters have been attributed to local photo-reduction of the silver ions combined to thermal diffusion, as illustrated in Eqs. (1)–(3). First the interaction of the infrared laser with the silver-containing glass frees electrons (Eq. (1)). The generation of a high free electron density in the glass enables the reduction of some silver ions to the atomic state (Eq. (2)). After more pulses inducing local heating a thermal diffusion of Ag^+ and Ag^0 occurs. The Ag^0 silver atoms diffuse towards silver ions leading to the formation of Ag_m^{x+} clusters (Eq. (3)).

Nevertheless, questions remain about the species involved in these processes. What is the ionization process? What is the free electron density? Which type of silver clusters are generated during the exposure? Which are implied in the luminescence properties of the photo-induced structures?

$$\text{Matrix} + h\upsilon \rightarrow e^- + h^+ \quad (1)$$

$$Ag^+ + e^- \rightarrow Ag^0 \quad (2)$$

....

$$xAg^+ + yAg^0 \rightarrow Ag_m^{x+} \qquad \text{with}(m = x + y) \quad (3)$$

Due to redissociation phenomena occurring at the center of the beam (where the irradiance is the highest), the clusters are mainly located at the periphery of the beam. Focusing the laser beam results in the formation of a luminescent pipe, which appears as a ring structure in the plane perpendicular to the propagation axis. Details on the formation of

* Corresponding author. Tel.: +33 5 4000 2543; fax: +33 5 4000 2761.
E-mail address: bourhis@icmcb-bordeaux.cnrs.fr (K. Bourhis).

the structures have already been reported in previous works [14,15] but the description of the local chemical composition is incomplete. Depicting the fundamental phenomena responsible for the structuring of the glass is necessary to understand the involved chemical reactions. Luminescence comparisons of the laser irradiations with other irradiation methods leading to similar emission spectra of the glass can also bring some information about the nature of the clusters.

In this paper, we report time-resolved measurements of laser-induced absorption in a silver and zinc phosphate radiophotoluminescent (RPL) glass through a transient absorption pump-probe experiment. From these data, the free electron density is deduced. The dynamics of the absorption process is also studied. Elements regarding the photo-induced modifications of the local glass composition following the femtosecond irradiation are herein revealed. Atomic force microscopy (AFM) and high resolution scanning electron microscopy (HR-SEM) investigations after acid etching of the irradiated zone have been performed. The emission spectra of the femtosecond exposed glasses are compared to those exhibited by γ- and electron-irradiated samples.

2. Experimental

2.1. Glass preparation

Melt-quenched glasses with $40P_2O_5$–$55ZnO$–$1Ga_2O_3$–$4Ag_2O$ (mol%) composition were prepared. $(NH_4)_2HPO_4$, ZnO, $AgNO_3$ and Ga_2O_3 in powder form were used as raw materials and mixed together with the appropriate amount in a platinum crucible. A heating rate of about 1 °C min^{-1} has been conducted up to 1000 °C. The melt was then kept at this last temperature (1000 °C) from 24 to 48 h. Following this step, the liquid was poured into a brass mold after a short increase of the temperature at 1100 °C in order to access the appropriate viscosity. The glass samples obtained were annealed at 320 °C (40 °C below the glass transition temperature) for 3 h, cut (0.5 to 1 mm-thick) and optically polished.

2.2. Sample exposure

Three different kinds of irradiation (femtosecond laser, γ rays and electron beam) were performed.

The setup for the laser irradiations is shown in Fig. 1. The laser is an Yb:KGW fiber laser system (t-Pulse 500, Amplitude Systemes) which delivers 470 fs, pulses at 1030 nm with a 9.44 MHz repetition rate. The maximum energy per pulse is 600 nJ. The femtosecond laser was focused using objectives with different numerical apertures (NA = 0.20 and 0.52) at a depth of 200 μm inside the glass. An acousto-optic modulator was used to adjust the number and/or the energy of the pulses. The glass was exposed to different irradiance levels, between 1.6 TW cm^{-2} (0.7 J cm^{-2}) to 3.1 TW cm^{-2} (1.5 J cm^{-2}), and different numbers of pulses, from 10^2 to 10^6. The irradiance is computed assuming Gaussian spatial and temporal profiles for the laser beam. The beam waist was estimated to be 1 μm. Laser-induced pipes perpendicular to the surface of the sample were written inside the glass with a length of 1 mm using a microprecision *xyz* stage. The refractive index modification threshold of this glass was previously determined and corresponds to an irradiance of about 2.8 TW cm^{-2} (fluence of 1.3 J cm^{-2}) [6].

γ irradiations were performed using a ^{60}Co source delivering 0.36 kGy h^{-1}.

Irradiations with a 20 kW accelerator delivering 15 μs electron pulses through a scanning beam (1–10 Hz) at a mean dose of 5 MGy h^{-1} were also performed.

2.3. Transient absorption experimental setup

The pump-probe experimental setup is depicted in Fig. 1b. A pump pulse and a probe pulse orthogonally polarized are generated via an interferometer containing two polarizing beam splitters. A mechanical chopper modulates the pump beam at a few kHz. A BBO crystal is inserted in the probe arm to generate the second harmonic of the laser (*i.e.* 515 nm). At the output of the interferometer, the sequence of the

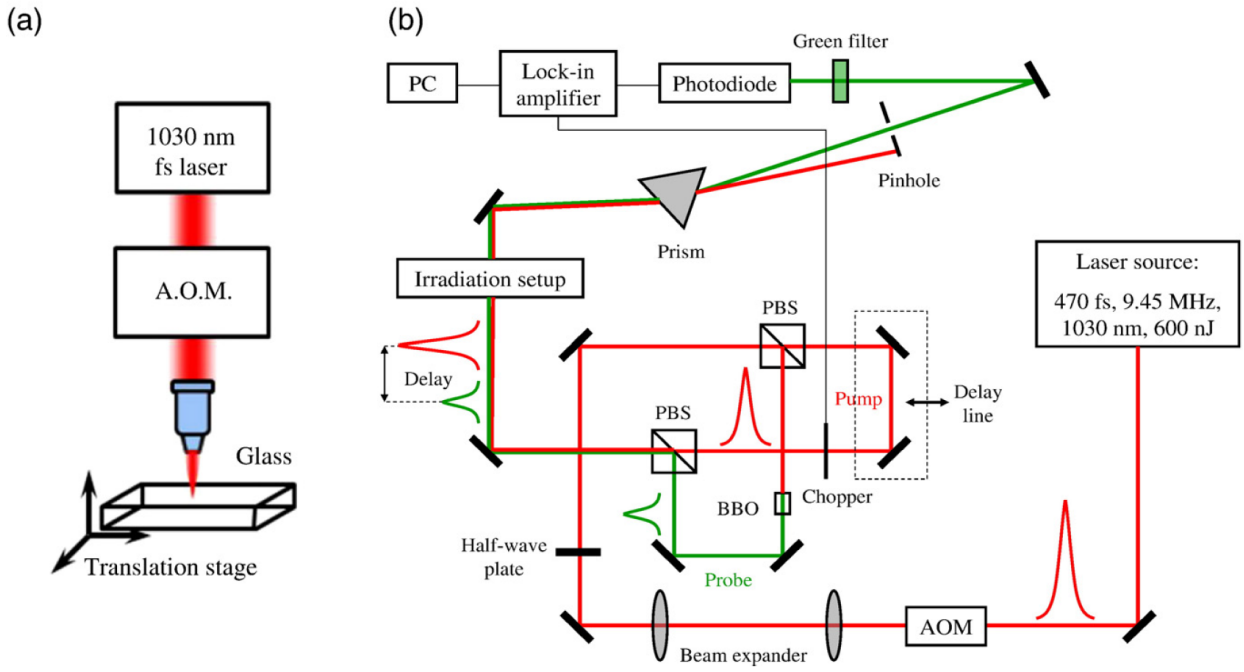

Fig. 1. (a) Laser irradiation setup and (b) Pump-probe transient absorption setup. AOM: Acousto-optic modulator, PBS: Polarizing beam splitter, BBO: β-barium borate doubling crystal, PC: Personal computer.

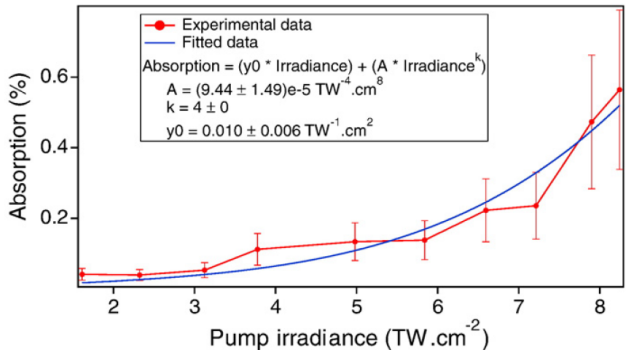

Fig. 2. Evolution of the absorption of the ionized material at zero delay versus the pump irradiance at the sample. The first term of the fitting equation is an offset due to thermal cumulative effects associated to the high repetition rate of the laser.

two pulses is focused (NA = 0.52) into the fixed sample, 200 μm below the surface and recollimated with another identical objective. The pump pulse is blocked with a pinhole combined to a prism and a green colored filter. The probe pulse is analyzed via a photodiode and a lock-in amplifier connected to the chopper. The data are collected with a computer. The delay line was moved over a distance corresponding to a 14 ps pump-probe delay during 1 s. Thus, the number of pulses on the sample for each acquisition was about 5×10^6. The pump irradiance was varied from 1.6 to 8.2 TW cm^{-2}, for which luminescent structures appear, and the probe irradiance was about 8 GW cm^{-2}. The temporal resolution of our experiment, defined as the cross-correlation of the pump and probe pulses, is about 700 fs.

2.4. Sample analysis

High resolution scanning electron microscopy (HR-SEM JEOL 6700F — gun field emission — resolution 1.1 nm) and atomic force microscope (AFM D.I. 3100 Veeco) were performed on the irradiated sample. In order to visualize the photo-induced structures an acid etching was performed with diluted HNO_3.

Luminescence spectroscopy of the photo-induced structures was performed on a SPEX VTM 300 Horiba Jobin-Yvon spectrophotometer. Confocal fluorescence microscopy was carried out at $\lambda_{exc} = 405$ nm on a Leica DMR TCS SP2 AOBS microscope equipped with a 40× objective and

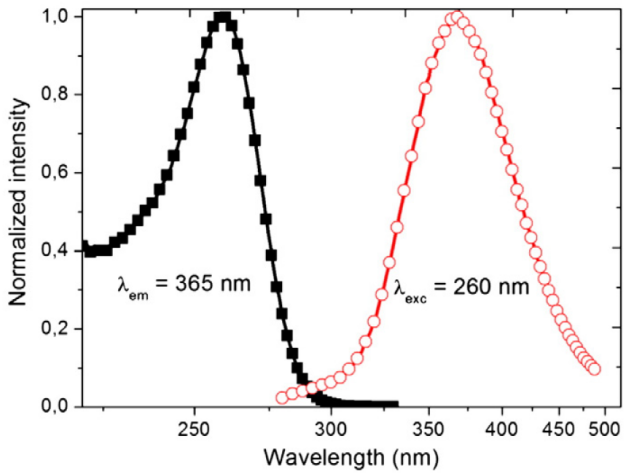

Fig. 3. Excitation spectrum ($\lambda_{em} = 365$ nm) and excitation spectrum ($\lambda_{exc} = 260$ nm) of the $40P_2O_5$–$55ZnO$–$1Ga_2O_3$–$4Ag_2O$ (mol%) glass. The bands correspond to the $5d^{10} \rightarrow 5d^9 4s^1$ transition of the Ag^+ isolated ion.

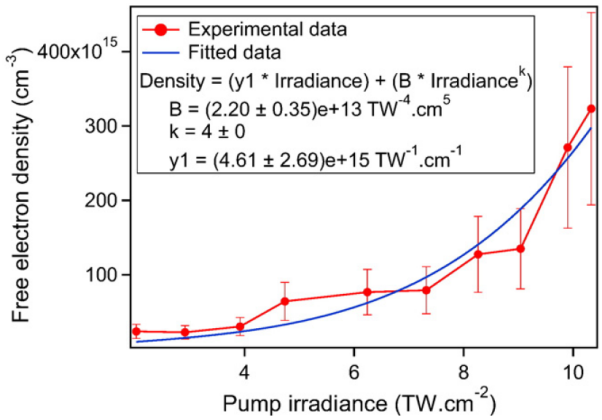

Fig. 4. Evolution of the free electron density versus the pump irradiance at the sample. The first term of the fitting equation is an offset due to thermal cumulative effects associated to the high repetition rate of the laser.

at $\lambda_{exc} = 325$ nm on a Labram HR-800 Horiba Jobin-Yvon spectrophotometer. No acid etching was used prior the luminescence analysis.

3. Results and discussion

3.1. Nonlinear absorption and luminescence properties of the pristine glass

The absorption of the pristine glass has been investigated as a function of the laser irradiance in order to determine the nonlinear absorption process. The maximum absorption, measured at zero delay, as a function of the pump irradiance is given in Fig. 2. In a multiphoton absorption regime, the absorption should scale as $A(I) \propto I^k$, where k is the order of the multiphoton process and I the irradiance. A fit with $k = 4$ gives a good agreement with the experimental data and provides that the four-photon absorption process is likely involved in the nanostructuring of the silver-containing RPL glass.

This multiphoton absorption behavior is confirmed by the calculation of the Keldysh parameter [16]. In our irradiation conditions (cut-off wavelength = 280 nm, laser wavelength = 1030 nm, refractive index = 1.58, maximum irradiance = 10 TW cm^{-2}), the Keldysh coefficient is about 1.88, which is higher than 1.5. We are therefore in a multiphoton ionization regime. As the irradiance decreases, the Keldysh coefficient gets higher and higher.

The pristine glass exhibits an absorption cut-off at around 270 nm mainly due to the silver ions associated absorption [15]. Luminescence

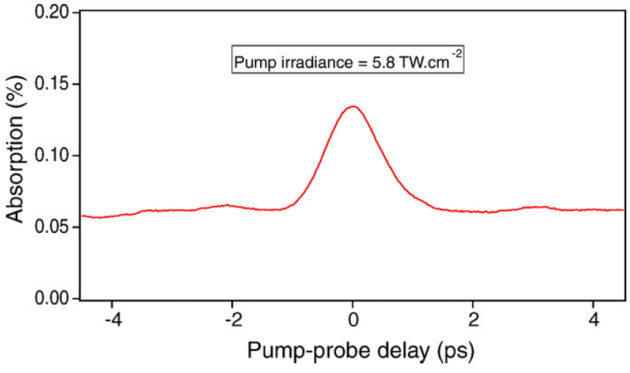

Fig. 5. Evolution of the absorption induced by the ionized material versus the pump-probe delay for a pump irradiance of 5.8 TW cm^{-2}. The curve is an average of 30 acquisitions. The standard deviation of these acquisitions gives an uncertainty of the measurements of 40%.

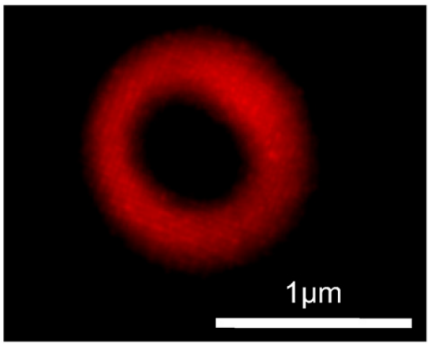

Fig. 6. Fluorescence confocal microscopy image ($\lambda_{exc}=405$ nm) of a photo-induced ring structure (at 1 MHz, NA = 0.52, deposited energy = 166 nJ).

properties of the pristine glass indicate as shown in Fig. 3 that the excitation at $\lambda_{exc}=260$ nm leads to a broad emission band at around 380 nm. The corresponding excitation spectrum for emission at $\lambda_{em}=365$ nm leads to a band centered at around 260 nm. Such emission has been attributed to the $d^{10}\rightarrow d^{9}s^{1}$ transition of the Ag^{+} silver isolated ions in the zinc phosphate matrix [17]. Since the four-photon wavelength (*i.e.* 1030/4 = 257 nm) is within the absorption band of the isolated Ag^{+} silver ions, one can assume that this transition is involved in the ionization process.

3.2. Free electron density

Assuming a simple Drude model [18,19] for the ionized material, the free electron density N_C can be determined from the absorption measurements as follow

$$N_C = \frac{cn_0\varepsilon_0 m_e}{e^2\tau_C L}\left(1+\frac{4\pi^2c^2\tau_C^2}{\lambda_0^2}\right)\ln\left(\frac{1}{T}\right) \quad (4)$$

Where c is the speed of light in vacuum, $n_0=1.58$ the refractive index of the glass at 1030 nm, ε_0 the dielectric permittivity in vacuum, m_e the electron rest mass, $\tau_c=0.4$ fs [20] the electronic collision time, $L=10$ µm the interaction length [21], λ_0 the laser wavelength and $T=1-A$ the transmission of the ionized material. As shown in Fig. 4, the measured free electron density ranges from 0.2 to 3×10^{17} cm^{-3}, and is four orders of magnitude below the critical electron density (*i.e.*

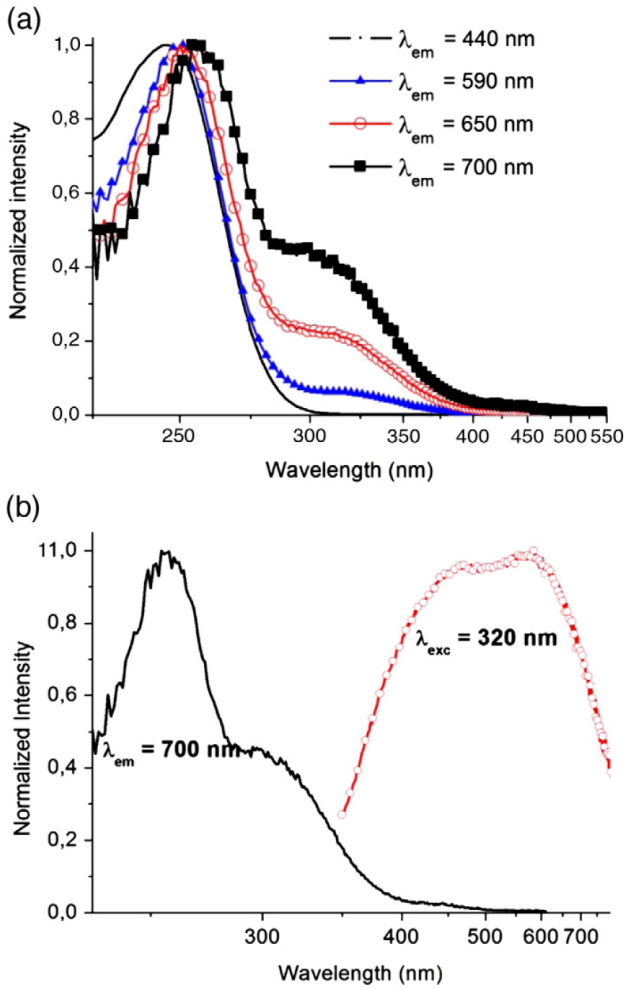

Fig. 7. (a) Excitation spectra at several emission wavelengths from $\lambda_{em}=440$ nm to 700 nm and (b) excitation ($\lambda_{em}=700$ nm) and emission ($\lambda_{exc}=320$ nm) spectra of the irradiated region. The dimension of the analyzed zone containing the pipes is about 1 mm^3 and contains structures induced under different irradiation conditions (at 1 MHz, NA from 0.20 to 0.52, deposited energy from 17 to 374 nJ).

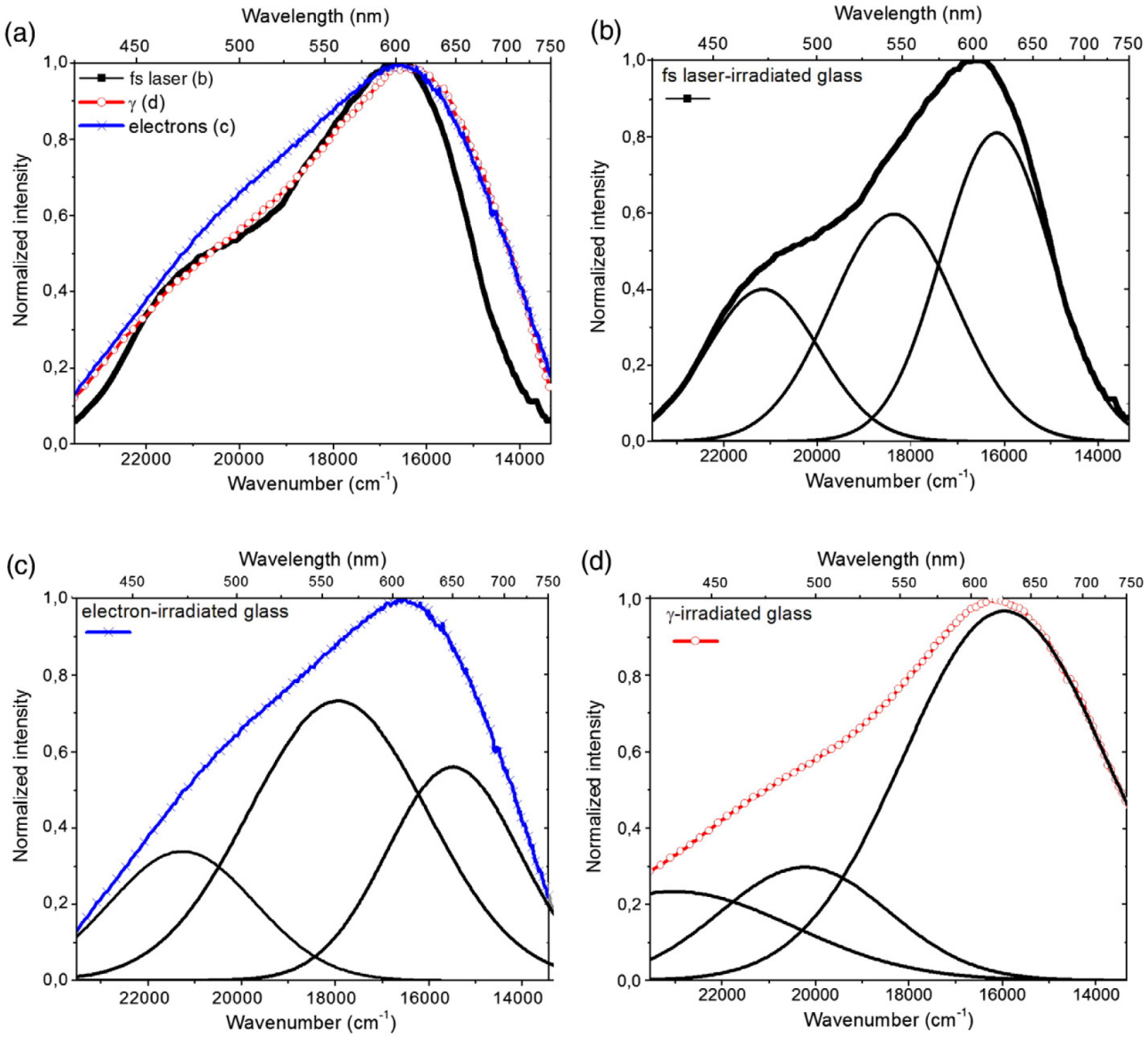

Fig. 8. (a) Emission spectra at $\lambda_{exc} = 325$ nm of (a) a femtosecond laser-irradiated structure (black line) at $I = 7.8$ TW cm^{-2}, number of pulses $= 10^7$, deposited energy ≈ 100 nJ, size of the ring ≈ 1.5 μm), a γ-irradiated glass (red line with circles) for a dose = 5.4 kGy and an electron irradiated glass (blue line with crosses) for dose = 30 kGy. Decomposition of the emission spectra of fs-laser (b), electron- (c) and γ- (d) irradiated glasses.

the electron density above which the ionized material is reflecting), which is about 10^{21} cm^{-3} at the laser wavelength.

3.3. Four-photon absorption coefficient and cross-section

To characterize the investigated RPL glass, it is interesting to determine two parameters related to its nonlinear absorption: the four-photon absorption coefficient and the four-photon absorption cross-section.

The four-photon absorption coefficient can be determined from the values of the free electron density as follow

$$\alpha_4 = \frac{4hc^2}{I_{pump}^4 \lambda_0^2} N_C \quad (5)$$

Where h is the Planck constant, c the speed of light in vacuum, I_{pump} the pump irradiance, λ_0 the laser wavelength and N_C the free electron density.

The four-photon absorption cross-section is given by

$$\sigma_4 = \left(\frac{hc}{\lambda_0}\right)^3 \frac{\alpha_4}{N} \quad (6)$$

Where h is the Planck constant, c the speed of light in vacuum, λ_0 the laser wavelength, α_4 the four-photon absorption coefficient and $N = 7.42 \times 10^{22}$ ions cm^{-3}, the total ionic concentration per unit volume.

Eqs. (5) and (6) give for the four-photon absorption coefficient and the four-photon absorption cross-section the following values, respectively:

$$\alpha_4 = (14.6 \pm 1.0).10^{-3}\,\text{cm}^5\,\text{TW}^{-3}$$

and

$$\sigma_4 = (14.1 \pm 1.0).10^{-118}\,\text{cm}^8\,\text{s}^3\,\text{photon}^{-3}$$

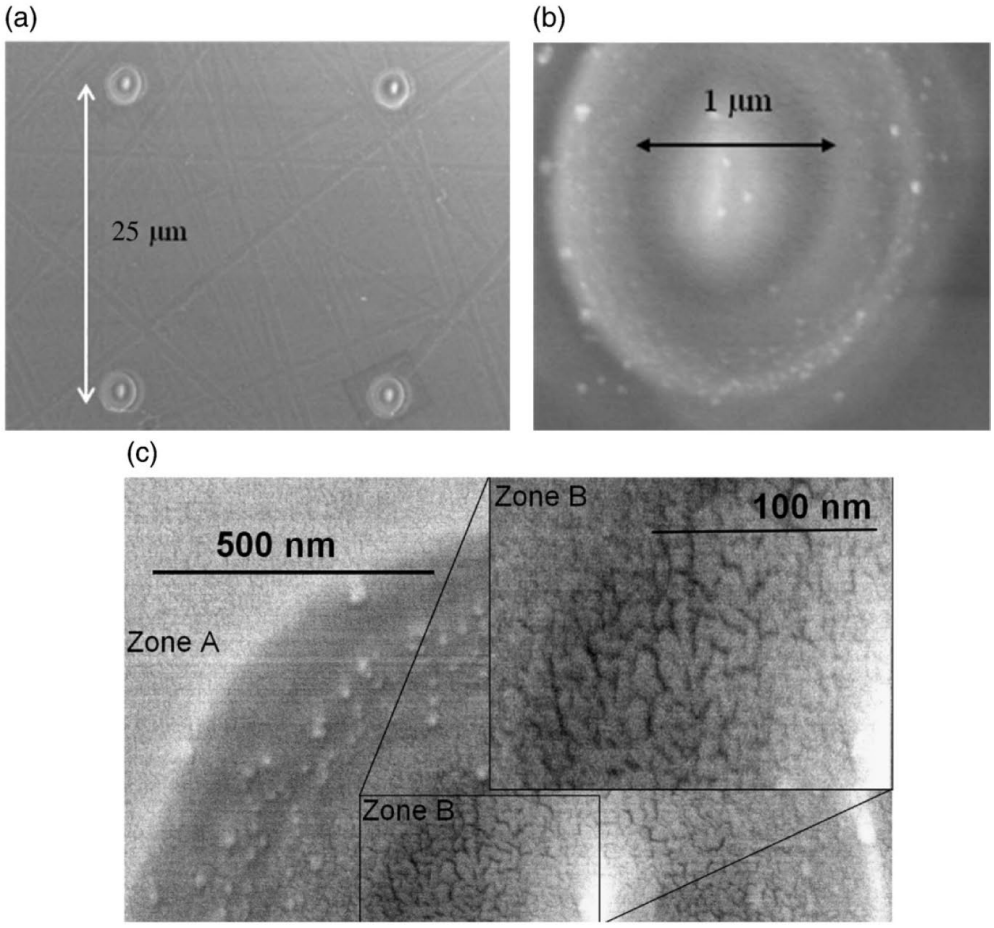

Fig. 9. (a) HR-SEM image of the laser irradiated region ($I = 9.8$ TW cm^{-2}, number of pulses $= 10^7$) after acid etching revealing the presence of micrometric photo-induced rings, (b) enlargement of a photo-induced structure and (c) zoom on the circular zone around the central peak of a photo-induced structure.

3.4. Dynamics of the absorption

A typical temporal dynamics of the absorption induced by the ionized material for a pump irradiance of 5.8 TW cm^{-2} is shown in Fig. 5. No absorption is present after 1.8 ps. Nevertheless, the temporal resolution of our experiment does not permit to reveal details below 700 fs. The absorption offset, which is about 0.05% at 5.8 TW cm^{-2}, is probably due to thermal cumulative effects associated to the high repetition rate of the laser.

3.5. Luminescence confocal spectroscopy

Fluorescence confocal microscopy revealed the presence of ring structures for an excitation at $\lambda_{exc} = 405$ nm. The width of the structure ranges from 1 to 15 µm depending on the irradiation conditions (numerical aperture, pulse energy, number of pulses) (Fig. 6).

Luminescence spectroscopy was carried out on the photo-induced structures. A first approach was to measure a macroscopic signal, *i.e.* a signal coming from multiple structures, using a fluorimeter. The excitation spectra reported in Fig. 7a show a band at 320 nm which is absent in the non-irradiated glass. An excitation in this band results in the emission of a broad band with visible maxima at 490 nm and 580 nm (Fig. 7b). Such bands can be associated to small Ag_m^{x+} silver clusters such as Ag_3^{2+} and Ag_4^{2+} for silver containing glasses [17,22,23]. No clear attribution of the absorption and emission bands has been given yet. In the excitation spectra (Fig. 7a), one can observe the band around 260 nm which corresponds to the intrinsic luminescence due to the isolated Ag^+ ions. The used fluorimeter does not allow a spatial separation between the non-irradiated and the irradiated zones. Indeed the size of the analyzed zone is about 1 mm^3 whereas the size of one pipe going from one side of the glass to the other one is estimated to be about 10^{-6} mm^3. That is why it was not possible to separate the signals emitted from the zones irradiated with various numerical apertures from 0.20 to 0.52. Nevertheless in the excitation spectra the relative intensity of the 320 nm band associated to the silver clusters increases for longer emission wavelengths proving that clusters are created.

Hence, going to a scale step further in the analysis is necessary. The emission spectrum on a single structure at $\lambda_{exc} = 325$ nm is reported in Fig. 8 using a confocal microscope in order to collect the signal corresponding to emission of a single ring structure. The emission spectrum obtained is quite different from the one obtained on multiple structures. A fluctuation of the ratio between the intensity of the bands at 540 nm and 620 nm seems to depend on both the irradiance and the number of pulses and is subject to current investigation. The emission spectrum of a single structure has been compared with the emission spectra of the γ- and electron-irradiated glasses. It has been reported that stable silver clusters are formed after γ irradiation in Li–Al–Ag–metaphosphate glasses [24] and in silver-doped sodium and calcium phosphates [25]. In γ-irradiated glasses, some clusters have been characterized thanks to their EPR signature especially Ag_m^{x+} with a low x/m ratio as Ag_3^{2+} and Ag_4^{3+}. Even though the mechanisms of formation of the clusters are different for the γ, electron and laser irradiations, comparisons of the resulting emission spectra can be performed. In any

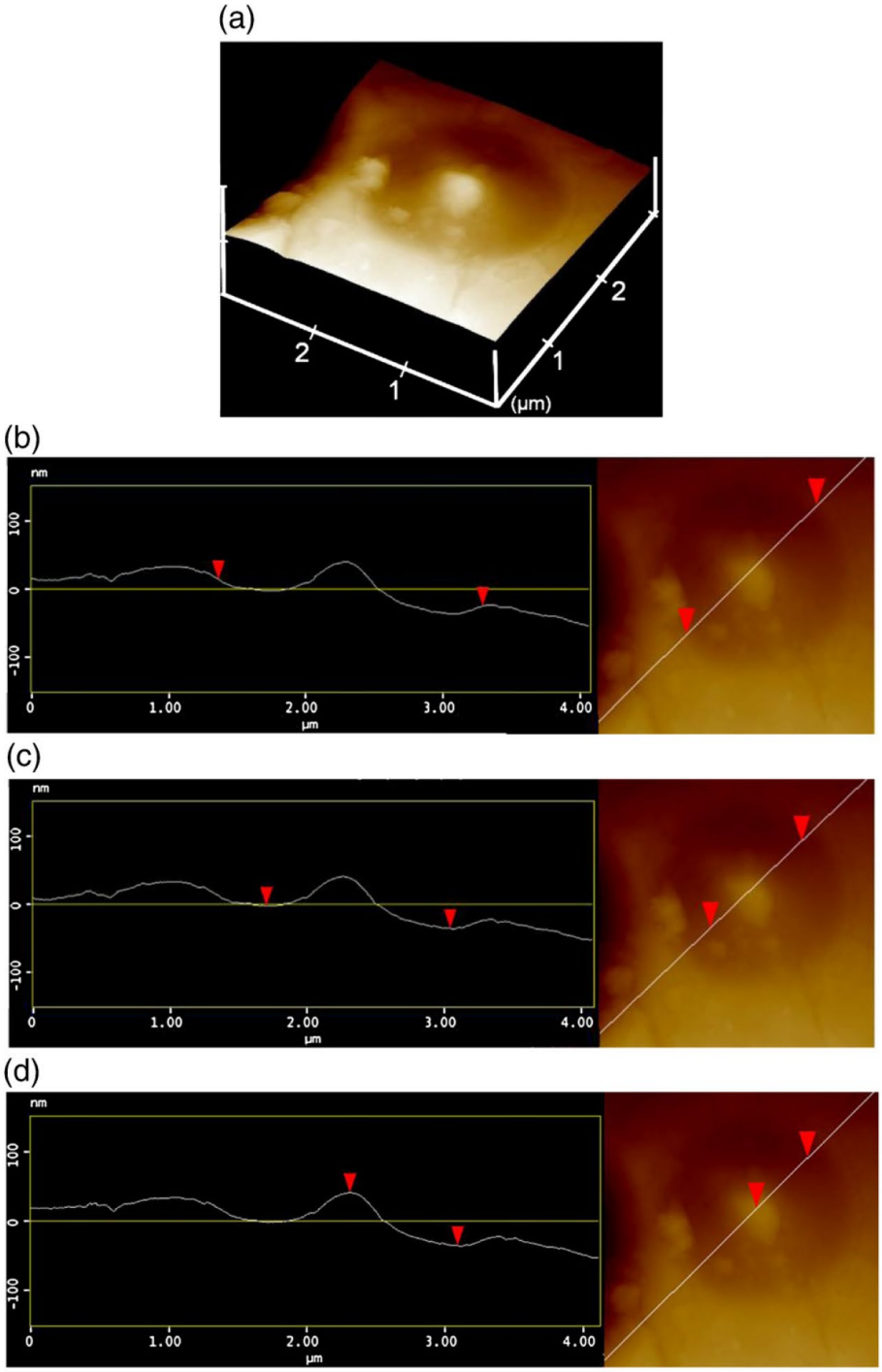

Fig. 10. (a) AFM reconstructed image of a photo-induced structure after acid etching. The distances between the two red triangles represent respectively (b) the total diameter of the fluorescent ring (see Fig. 6), (c) the diameter of the black ring (see Fig. 9b) and (d) the depth of the acid etching.

case, using an exponential summation approach, three different components can be isolated at around 440–480 nm, 500–560 nm and 620–650 nm. In the case of electron and laser irradiations, the two first bands are more intense than for the γ-irradiated sample. In the case of laser irradiation, the increase of the dose induces the relative intensity of the band located at around 500–560 nm. Such results have been already observed also for γ-irradiated glasses. At low dosage, only the band above 600 nm is visible [16]. Such behavior for high dosage should be related to the formation of larger amount of Ag^0 electron traps and so with the formation of different clusters Ag_m^{x+} with a decreasing x/m ratio.

The emission data indicate that even if the formation mechanism is different, the resulting clusters are similar and one can suspect at least two different silver cluster species.

3.6. AFM and HR-SEM microscopy

After polishing to bring the photo-induced structures at the surface and soft HNO_3 acid etching, HR-SEM (Fig. 8a) showed a higher reactivity to the acid of the photo-induced structures than of the surrounding matrix. Imaging with a higher magnification (Fig. 8b) reveals a white circular shape of about 2 μm at the periphery, surrounding a black circle of about 1 μm. The observed structures were correlated to the size of the luminescent structures previously observed by Bellec et al. [14]. The center of the photo-induced structure appears white on the HR-SEM images in Fig. 9a and b which could be partially assigned to a topographic variation.

Fig. 10a shows an AFM reconstruction of the same structure. The circular shape can be clearly identified. Cross-sections of the structure are presented in Fig. 10. The level difference between the left side and the right side of the cross-section is related to the non-flatness of the sample. However the dimensions of the structure can be extracted and correlated to those measured in the HR-SEM images. The total width of the structure obtained by AFM is 1.8 μm (Fig. 10b). One can observe that the etching is maximal at about 500 nm from the center leaving a central peak surrounded by valley. The distance between the deepest points is 1.2 μm (Fig. 10c). The height difference between the highest point and the lowest point indicates that the acid etching was optimized and removed only 80 nm of matter (Fig. 10d). Such an acid attack makes the optical visualization of the structure possible and enables the analysis of the photo-induced structures using HRSEM.

By looking more in details inside the circular zone around the central peak, one can observe that the glass is not homogeneously affected by the acid etching (Fig. 9c). Indeed out of the photo-induced structure (Zone A), no damage of the surface is observed. On the contrary the etched zone shows small irregularities when approaching the peak. The zoom on the very neighborhood of the peak (Zone B) reveals surface defects which look like porous material. Since the luminescent ring is also located in this region, one can suspect that this zone has been strongly affected by silver migration leading to a weakening of the glass structure and to bonds breakings. Some studies on semiconductor materials [26–28] have also shown that the interaction of ultrafast pulsed lasers and crystalline matter was leading to the generation of a high free electron density, leading to materials chemical modifications. A lower electron density seems in the silver and zinc phosphate glass to result in modifications of the porosity and silver migration. Analysis using X-ray microprobe on a larger pipe (6 μm-wide) obtained by depositing more energy (≈200 nJ) than for the 1 μm-wide structures has allowed the detection of a lower silver content in the depth of the acid etched zone. It tends to prove that a silver migration has occurred during the laser irradiation. The acid selectivity seems then related to this silver migration. Further experiments are currently carried out in order to correlate the images collected by HR-SEM, AFM and micro-luminescence experiments.

4. Conclusion

Submicrometer luminescent pipes have been obtained in a silver zinc phosphate glass due to local formation of Ag_m^{x+} silver clusters following the creation of electron traps. The free electron density has been measured for different irradiation conditions and has been found to be about four orders of magnitude lower than the critical density. A four-photon absorption process is likely involved in the electron trapping mechanism necessary for the nanostructuring of these glasses.

The luminescence of these structures compared to that of γ- and electron-irradiated glasses has shown that similar luminescent clusters are formed under laser irradiation. Three contributions to the emission spectra have been identified due to different Ag_m^{x+} species. The acid etching prior observation using HR-SEM and AFM has revealed different local chemical contrasts in the irradiated area. Preliminary results indicate a composition variation between the center and the ring regions, leading to a deeper etching where the silver content is affected.

Acknowledgments

The authors acknowledge S. Gomez and the CREMEM platform (ICMCB-CNRS University of Bordeaux) for the HRSEM images, C. Labrugère and the CECAMA (ICMCB-CNRS-University of Bordeaux) for the AFM measurements, and P. Legros, C. Poujol and the BIC platform (Neurosciences Institute of the University of Bordeaux) for the confocal fluorescence microscopy. This work has been supported by the "GIS Advanced Materials in Aquitaine", the Region Aquitaine, a FACE grant from the French Embassy in the US and the IMI-NFG (NSF grant No. DMR-0409588).

References

[1] R.R. Gattass, E. Mazur, Nat. Photonics 2 (4) (2008) 219–225.
[2] Y. Shimotsuma, K. Hirao, J. Qiu, K. Miura, J. Non-Cryst. Solids 352 (2006) 646–656.
[3] J. Gottmann, D. Wortmann, M. Hörstmann-Jungemann, Appl. Surf. Sci. 255 (10) (2009) 5641–5646.
[4] M. Rosenbluh, I. Antonov, D. Ianetz, Yu. Kaganovskii, A.A. Lipovskii, Opt. Mater. 24 (2003) 401–410.
[5] E.N. Glezer, M. Milosavljevic, L. Huang, R.J. Finlay, T.-H. Her, J.P. Callan, E. Mazur, Opt. Lett. 21 (24) (1996) 2023–2025.
[6] L. Canioni, M. Bellec, A. Royon, B. Bousquet, T. Cardinal, Opt. Lett. 33 (4) (2008) 360–362.
[7] A.V. Dotsenko, A.L. Diikov, T.A. Vartanyan, Sens. Actuators B 94 (2003) 116–121.
[8] S.D. Stookey, Photosensitive glass, Ind. Eng. Chem. 41 (4) (1949) 856–861.
[9] T. Tani, "Photographic Sensitivity: Theory and Mechanisms", ed. by Oxford University Press (Oxford, 1995), p.142.
[10] K. Becker, At. Energy Rev. 5 (1967) 43–95.
[11] V.A. Borgman, Y.P. Kostikov, A.V. Amosov, Fiz. Khim. Stekla 7 (1) (1981) 103–106.
[12] H. Vogel, K. Becker, Nukleonik 12 (7) (1965) 18–33.
[13] H. Schneckenburger, D.F. Regulla, E. Unsöld, Appl. Phys. A 26 (1981) 23–26.
[14] M. Bellec, A. Royon, B. Bousquet, K. Bourhis, M. Treguer, T. Cardinal, M. Richardson, L. Canioni, Opt. Express 17 (12) (2009) 10304.
[15] C. Maurel, T. Cardinal, M. Bellec, L. Canioni, B. Bousquet, M. Treguer, J.J. Videau, J. Choi, M. Richardson, J. Lumin. 129 (12) (2009) 1514–1518.
[16] L.V. Keldysh, Sov. Phys. JETP 20 (1965) 1307–1314.
[17] I. Belharouak, C. Parent, B. Tanguy, G. Le Flem, M. Couzi, J. Non-Cryst. Solids 244 (1999) 238–249.
[18] P. Drude, Ann. Phys. 306 (3) (1900) 566.
[19] P. Drude, Ann. Phys. 308 (11) (1900) 369.
[20] V.V. Temnov, K. Sokolowski-Tinten, P. Zhou, A. El-Khamhawy, D. von der Linde, Phys. Rev. Lett. 97 (2006) 237403.
[21] We assume the interaction length is on the same order of magnitude as the confocal parameter $b = 2\frac{\pi n_0 w_0^2}{\lambda_0}$.
[22] A.V. Podlipensky, V. Grebenev, G. Seifert, H. Graener, J. Lumin. 109 (2004) 135–142.
[23] Y. Dai, X. Hu, C. Wang, D. Chen, X. Jiang, C. Zhu, B. Yu, J. Qiu, Chem. Phys. Lett. 439 (2007) 81–84.
[24] R. Yokota, H. Imagawa, J. Phys. Soc. Jpn 23 (5) (1966) 1038–1048.
[25] A.V. Dmitryuk, S.E. Paramzina, A.S. Perminov, N.D. Solov'eva, N.T. Timofeev, J. Non-Cryst. Solids 202 (1996) 173–177.
[26] A. Rousse, C. Rischel, S. Fourmaux, I. Uschmann, S. Sebban, G. Grillon, P. Balcou, E. Foerster, J.P. Geindre, P. Audebert, J.-C. Gauthier, D. Hulin, Nature 410 (2001) 65–68.
[27] C.W. Siders, A. Cavalleri, K. Sokolowski-Tinten, Cs. Tóth, T. Guo, M. Kammler, M. Horn von Hoegen, K.R. Wilson, D. von der Linde, C.P.J. Barty, Science 286 (5443) (1999) 1340–1342.
[28] C. Rose-Petruck, R. Jimenez, T. Guo, A. Cavalleri, C.W. Siders, F. Rksi, J.A. Squier, B.C. Walker, K.R. Wilson, C.P.J. Barty, Nature 398 (1999) 310–312.